JOURNAL OF Applied Polymer SCIENCE

Batch foaming of carboxylated multiwalled carbon nanotube/poly(ether imide) nanocomposites: The influence of the carbon nanotube aspect ratio on the cellular morphology

Haitao Yu,[1] Yajie Lei,[2] Xuejiang Yu,[2] Xianzhong Wang,[2] Tao Liu,[2] Shikai Luo[1,2]

[1]Material Science and Engineering College, Southwest University of Science and Technology, Mianyang 621010, Sichuan, China
[2]Institute of Chemical Materials, China Academy of Engineering Physics, Mianyang 621900, Sichuan, China
Correspondence to: T. Liu (E-mail: liutao_caep@163.com) and S. Luo (E-mail: luosk_caep@163.com)

ABSTRACT: A series of microcellular poly(ether imide) (PEI) foams and nanocellular carboxylated multiwalled carbon nanotube (MWCNT-COOH)/PEI foams were prepared by the batch foaming method. MWCNT-COOHs with different aspect ratios were introduced into the PEI matrix as heterogeneous nucleation agents to improve the cell morphology of the microcellular PEI foams. The effect of the aspect ratio of the MWCNT-COOHs on the cellular morphology, and gas diffusion is discussed. The results show that with the addition of MWCNT-COOH, the sorption curve showed a slight reduction of carbon dioxide solubility, but the gas diffusion rate could be improved. The proper aspect ratio of MWCNT-COOH could improve the cellular morphology under the same foaming conditions, in which *m*-MWCNT-COOH (aspect ratio $\approx$ 1333) was the best heterogeneous nucleation agent. When the foaming temperature was 170°C, the cell size and cell density of nanocellular *m*-MWCNT-COOH reduced to 180 nm and increased to 1.58 $\times 10^{13}$ cells/cm^3, respectively. © 2015 Wiley Periodicals, Inc. J. Appl. Polym. Sci. **2015**, *132*, 42325.

KEYWORDS: composites; foams; graphene and fullerenes; nanotubes; porous materials

Received 8 December 2014; accepted 6 April 2015
DOI: 10.1002/app.42325

INTRODUCTION

A *microcellular foam* is defined as a foam having average cell diameters in the range of 1–10 μm and cell densities on the order of 10^9-10^{15} cells/cm^3. Microcellular foams were invented at the Massachusetts Institute of Technology under the direction of Professor Nam P. Suh[1] and have been studied extensively for the past 20 years.[2–4] Because of its high strength-to-weight ratio, excellent heat and sound insulation, high energy or mass absorption, and material-saving properties, microcellular foams have attracted significant attention.[5–12]

Carbon-based nanoparticles possess an even higher nucleation efficiency than nanoclays because of the lower contact angle among the particles, polymer matrix, and gas;[13] they can act as effective heterogeneous nucleation agents to improve the cell morphology of microcellular foams. Carbon nanotubes (CNTs), a kind of carbon-based nanoparticles, have generated huge activity in most areas of science and engineering because of their unprecedented physical and chemical properties since their discovery in 1991,[14,15] so CNTs have been widely used in foaming fields. For example, Zhai *et al.*[16] found that in the poly (ethylene-co-octene) (PEOc)/multiwalled nanotube (MWNT) system, the MWNTs tended to orient in the cell wall compared with the way they did in the neat PEOc foams. The MWNTs acted as a self-reinforcing element, protecting the cells from destruction during cell growth. Ameli *et al.*[17] demonstrated nanocellular/microcellular PP/multiwalled carbon nanotube (MWCNT) composites exhibiting a higher conductivity, lower electrical percolation, higher dielectric permittivity, and lower dielectric loss; these could be used for electromagnetic shielding and charge storage application. Chen *et al.*[9] investigated the effect of different lengths of MWCNTs on nucleation and found that nucleation occurred mainly at the nanotube ends rather than at the sidewalls at low saturation pressure. At high saturation pressures, nucleation was in favor of the higher aspect ratio MWCNT nanocomposites. However, the poor solubility and processability caused by their inherent attractive van der Waal's interactions between nanotubes made CNTs aggregate and exist as bundles in the native state,[18] and this had an important effect on the nucleation.

Poly(ether imide) (PEI) is one of the most important high-performance engineering thermoplastics; they have been extensively used in commercial applications because of their excellent thermal stability, remarkable tensile strength, electrical

Table I. Parameters of the MWCNT-COOH Samples

Type of MWCNT-COOH	Length (μm)	Diameter (nm)	Average aspect ratio	Tap density (g/cm^3)	True density (g/cm^3)
s-MWCNT-COOH	10–30	<8	2500	0.27	2.1
m-MWCNT-COOH	10–30	10–20	1333	0.22	2.1
t-MWCNT-COOH	10–30	20–30	800	0.28	2.1

s-MWCNT-COOH = diameter of CNT is much shorter (8 nm); *m*-MWCNT-COOH = diameter is middle; *t*-MWCNT-COOH = diameter is thicker than *s*-MWCNT-COOH and *m*-MWCNT-COOH.

insulating properties, wear-resistance property, dimensional stability, flame resistance, and so on. So far, there have been few investigations on microcellular foams based on PEI with the batch foaming method.[19–23] However, there has been lack of articles reported systematically on the effect of CNT on the nucleation of microcellular CNT/PEI foams.

It is known that the carboxyl group has a high carbon dioxide (CO_2) affinity; this could improve the wettability of CO_2 on the CNTs, lead to a lower contact angle of CO_2 on the MWCNT surface, and enhance the heterogeneous nucleation efficiency. At the same time, carboxylated multiwalled carbon nanotubes (MWCNT-COOHs) can improve dispersion in the nanocomposite materials.[24] In this study, a series of microcellular and nanocellular MWCNT-COOH/PEI foams were prepared by the batch foaming method. MWCNT-COOHs with different aspect ratios were introduced into the PEI matrix as heterogeneous nucleation agents to improve the cell morphology of microcellular PEI foams. Keeping the length of MWCNT-COOH constant, we systematically examined the effect of the aspect ratio of the MWCNT-COOHs on the cellular morphology.

EXPERIMENTAL

Materials

PEI (Ultem 1100) was supplied by SABIC, Saudi Arabia. The density of amorphous PEI was 1.24 g/cm^3. Three different diameters of MWCNT-COOH with the same lengths (10–30 μm) were supplied by Chengdu Organic Chemicals Co., Ltd. (China). The parameters of MWCNT-COOH are shown in Table I.

Preparation of the MWCNT-COOH/PEI Nanocomposite Films

PEI nanocomposites with 1 wt % MWCNT-COOH were processed in a PTW252 twin-screw extruder (Haake, Germany) to give samples. All of the samples were dried at 140°C for 4 h to remove residual moisture. Then, a blow membrane with a thickness of 0.45 mm was squeezed by a film-blowing machine (Haake, Germany). All of the films were cut into 12.3 × 45.5 mm^2 specimens for absorption, desorption, and foaming studies.

Gas Saturation and Desorption

The absorption and desorption of CO_2 in the PEI and MWCNT-COOH/PEI nanocomposite films were investigated. The saturation time and temperature were controlled to vary the amount of gas delivered into the PEI matrix. CO_2 (99% pure) was supplied by Changjun Gas Co., Ltd. (China).

The saturation pressure was set to 8 MPa, and the saturation temperatures were 40, 50, 60, and 70°C, respectively. During the saturation process, specimens were periodically removed from the pressure vessel and weighed (sensitivity = 0.1 mg) to measure the gas uptake. The specimens were then promptly returned to the pressure vessel and repressurized. The time needed for weighing the specimens was sufficiently short compared to the time needed to achieve full saturation, so the error introduced in the gas-uptake measurements could be neglected.

Desorption experiments were conducted at room temperature (~26°C) and atmospheric pressure. Periodic mass measurements were taken to record the amount of gas dissolved in the sample.

Foaming with Supercritical Fluid Carbon Dioxide ($scCO_2$)

PEI and their nanocomposite films were foamed by a high-pressure self-developed batch foaming device with $scCO_2$ as the blowing agent under different foaming conditions. The vessel was flushed with low-pressure CO_2 for about 2 min, and then, the pressure was increased to 8 MPa. After the samples were saturated in $scCO_2$ for 23 h to achieve equilibrium saturation, they underwent a rapid quenching of pressure, were removed from the pressure vessel, and were placed into a temperature-controlled hot silicon oil bath to foam. Then, they were immediately moved into an ice–water bath to fix the morphology of the samples. Any excess oil was removed from the surface of the samples by tissue. The foaming temperatures were set to 150, 160, 170, and 180, and the foaming times were set to 5, 15, 25, 35, 45, 55, and 65 s, respectively.

Cell morphology was observed with an Apollo 300 scanning electron microscope. The samples were scored with a razor blade and freeze-fractured in liquid nitrogen, and the fractured surface was sputter-coated with gold. Cell size and cell density analysis was conduced with ImageJ software. For each micrograph, more than 100 bubbles was necessary. The cell density (N_0),the number of cells per cubic centimeter of the foams, was calculated with eq. (1):

$$N_0 = \left(\frac{nM^2}{A}\right)^{3/2}\left(\frac{1}{1-V_f}\right) \quad (1)$$

where n is the number of cells in the picture, M is the magnification factor, A is the area of the scanning electron microscopy (SEM) picture in square centimeters, and V_f is the void fraction of the foamed sample. It was defined as follows:

$$V_f = 1 - \frac{\rho_f}{\rho} \quad (2)$$

where ρ_f is the density of the bulk foam and is determined according to the provision ASTM D 792 of the American Society for Testing and Materials and ρ is the density of the unfoamed material.

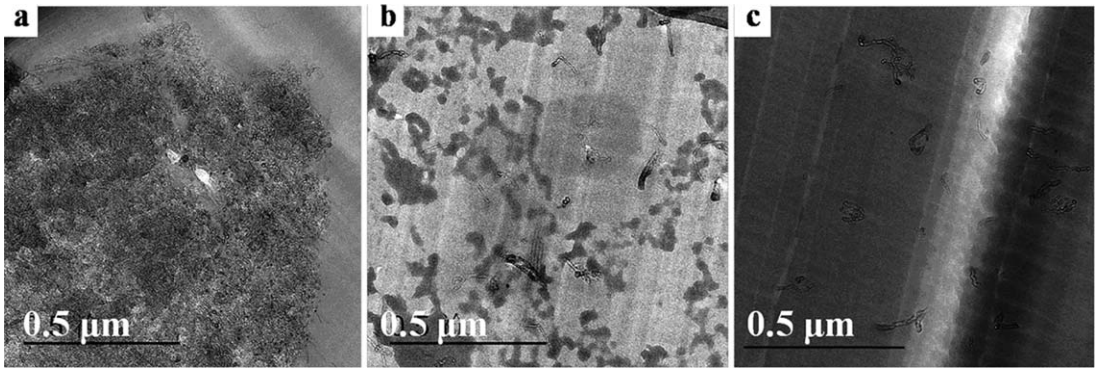

Figure 1. Typical transmission electron microscopy images of the MWCNT-COOH/PEI nanocomposites: (a) *s*-MWCNT-COOH/PEI, (b) *m*-MWCNT-COOH/PEI, and (c) *t*-MWCNT-COOH/PEI.

RESULTS AND DISCUSSION

Dispersion of the MWCNT-COOHs in PEI

Typical transmission electron microscopy images of the nanocomposites are shown in Figure 1. The images indicate the good dispersion of *m*-MWCNT-COOHs and *t*-MWCNT-COOHs in the PEI matrix, no agglomerates were observed, whereas *s*-MWCNT-COOHs were aggregated to bundles composed of hundreds of individual nanotubes. *s*-MWCNT-COOHs probably had a higher aspect ratio than *m*-MWCNT-COOHs and *t*-MWCNT-COOHs.

Transmission electron microscopy (TEM) was used to investigate the dispersion of MWCNT-COOH in PEI. The samples were microtomed at room temperature with a diamond knife at a thickness of 100 nm and mounted on a 200-mesh copper grid. Images were observed with a Zeiss Libra 200 FE using an accelerating voltage of 200 kV.

Gas Sorption and Desorption

Figure 2 shows the gas uptake in units of milligrams of CO_2 per gram of neat PEI, *s*-MWCNT-COOHs, *m*-MWCNT-COOHs,

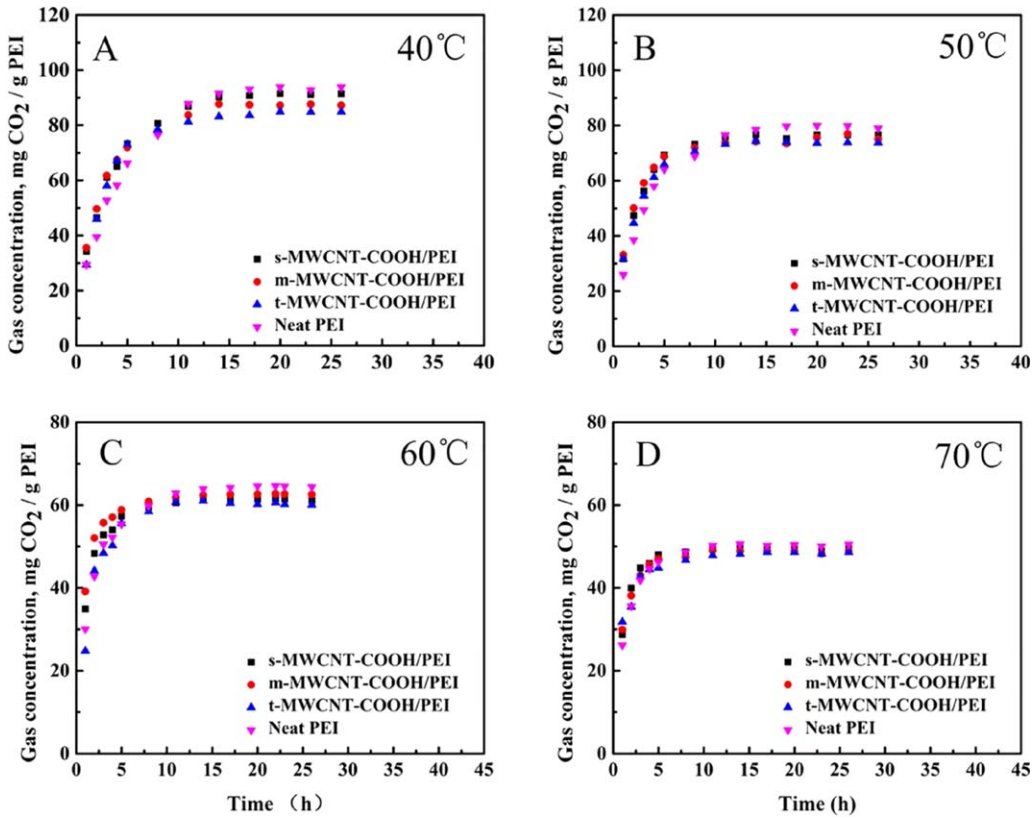

Figure 2. Plots of CO_2 uptake for the neat PEI, *s*-MWCNT-COOH, *m*-MWCNT-COOH, and *t*-MWCNT-COOH as a function of time at different temperatures: (A) 40, (B) 50, (C) 60, and (D) 70°C. The data are for 0.45 mm thick specimens, and the saturation pressure was 8 MPa. [Color figure can be viewed in the online issue, which is available at wileyonlinelibrary.com.]

and *t*-MWCNT-COOHs, respectively, as a function of time at various saturation temperatures of 40, 50, 60, and 70°C, respectively. All of the saturation pressures were 8 MPa.

With increasing saturation temperature, the gas saturation concentration decreased, but the gas diffusivity increased. The gas concentration increased rapidly at the beginning of 5 h then leveled off after 23 h. The absorbed gas concentration of *m*-MWCNT-COOH/PEI was the highest at first, but the equilibrium of the neat PEI became much higher than those of the other samples. However, the absorbed gas concentrations of the *s*-MWCNT-COOH/PEI and *m*-MWCNT-COOH/PEI nanocomposites did not exhibit significant differences because PEI contained carbonyl groups, which acted as electron donors and exhibited specific interactions with CO_2 as electron acceptors rather than as electron donors.[25] Although the MWCNT-COOH induced the carboxyl groups, the content of the carboxyl group was low, and the main structure of the MWCNT-COOHs was still the MWCNTs. When MWCNT-COOHs were added in the PEI matrix, the MWCNT-COOHs occupied the space but did not have $scCO_2$ absorption capacity and hindered the PEI matrix in the absorbance of CO_2. However, with the addition of the MWCNT-COOHs, the MWCNT-COOHs could form the path of CO_2; this improved the gas diffusion rate. Both equilibrium time and the saturation concentration of CO_2 decreased with decreasing saturation temperature. This was attributed to the movement of the molecular chain and the decrease in the solubility of the blowing agent CO_2. As the temperature of $scCO_2$ increased, the movement of the molecular chain may have improved the gas diffusion rate and resulted in a decrease in the equilibrium time of gas absorption. At a constant pressure, the unit volume molar concentration of CO_2 decreased with the growth of temperature according to the gas equation of state as follows:

$$PV = nRT \tag{3}$$

where P is the pressure of gas; V and T are the volume and temperature, respectively; and R is a constant. With decreasing unit volume molar concentration of CO_2, the PEI matrix decreased the CO_2 differential concentrations inside and outside; this resulted results in a decrease in the saturation concentration. When the amount of CO_2 absorbed in PEI increased, the heterogeneous nucleation efficiency increased.[19] Therefore, the parameters of $scCO_2$ were set to a saturation temperature of 40°C and a saturation time of 23 h; this made the matrix have the highest amount of CO_2 in this study.

Compared with a sorption model,[26] which studies the upper limit of the equilibrium concentration at specific temperature and saturation pressure, the equilibrium concentration data described in this article was much lower than the theoretical value. At a 40°C saturation temperature, for instance, the theoretical upper limit of the equilibrium concentration was 12.3 wt %, whereas the actual value was 9.4 wt %. This may have been due to the fact that the specimens contained moisture before they were put into the vessel, and the saturation temperature could not evaporate it absolutely; this led to a relative reduction in the amount of CO_2. As shown in Figure 3, the gas concentration could not approach zero when the desorption equilibrium was reached after 70 h; this indicated that the saturated films still had significant amounts of CO_2 in the test specimen. Meanwhile, the desorption data revealed that the desorption rate of CO_2 in the early stage was higher than that of CO_2 in the final stage.

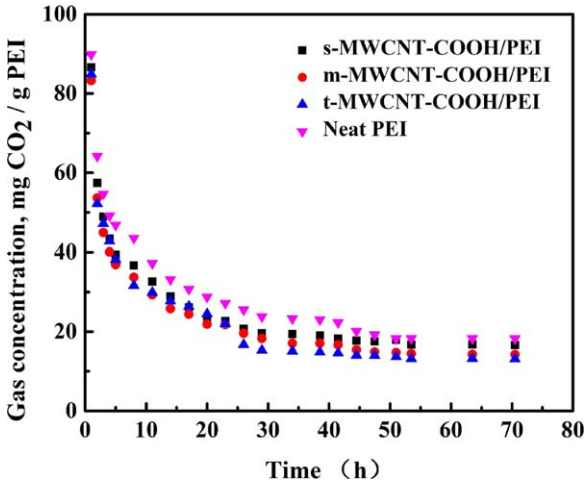

Figure 3. Plots of the CO_2 concentration as a function of the desorption time for the neat PEI, *s*-MWCNT-COOH, *m*-MWCNT-COOH, and *t*-MWCNT-COOH at 26°C. [Color figure can be viewed in the online issue, which is available at wileyonlinelibrary.com.]

Influence of the Aspect Ratio of MWCNT-COOH on the Cell Morphology

The cell nucleation process is commonly described by classical nucleation theory, and the ends of MWCNT-COOHs have a so-called nanoscale cylindrical pore structure, which may trap CO_2-forming gas cavities, and nucleation favors the ends of nanotube. Preexisting gas cavities can lower the critical free energy of nucleation drastically and facilitate rapid bubble nucleation.[24] In this study, the nanocomposites contained three types of 1 wt % MWCNT-COOHs with the same length but different diameters. As the diameters of the MWCNT-COOHs were all on the nanoscale and loaded with the same concentration, we speculated that they had the same ends but different diameters.

According to classical nucleation theory, the difference in chemical potentials is the mechanical and thermodynamic driving force for the nucleation growth of cells. The energy barrier that a nuclei should overcome to grow into a bubble, the homogeneous nucleation, is described by eq. (4):

$$\Delta G^*_{\text{hom}} = \frac{16\pi}{3\Delta p^2}\gamma^3 \tag{4}$$

where ΔG^*_{hom} is critical free energy of homogeneous bubble nucleation, γ is the interfacial tension of the polymer matrix/CO_2 mixture and Δp is the pressure drop during foaming. Similarly, the rate of heterogeneous nucleation could be expressed by eq. (5):

$$\Delta G^*_{\text{het}} = \Delta G^*_{\text{hom}} \frac{f(m,w)}{2} \tag{5}$$

where ΔG^*_{het} is critical free energy of heterogeneous bubble nucleation, where m is contact angle and it is concerned with

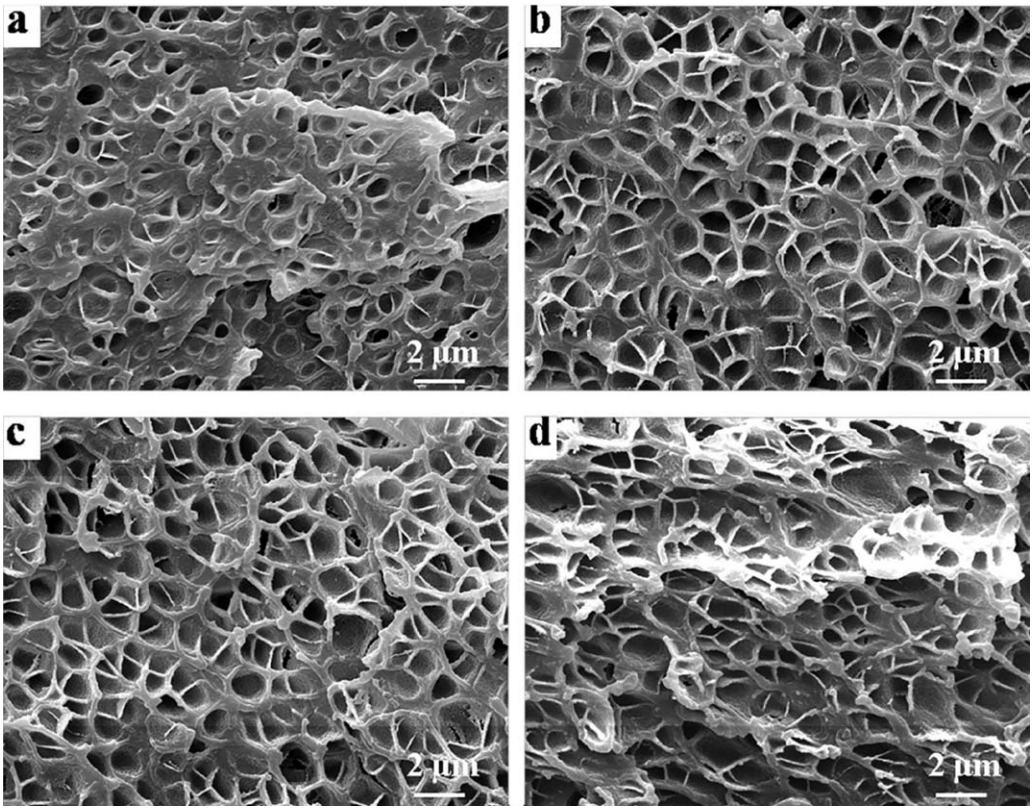

Figure 4. SEM images of the neat PEI foams at 180°C with different foaming times: (a) 5, (b) 15, (c) 25, and (d) 35 s (magnification 6000×, scale bar = 2 μm).

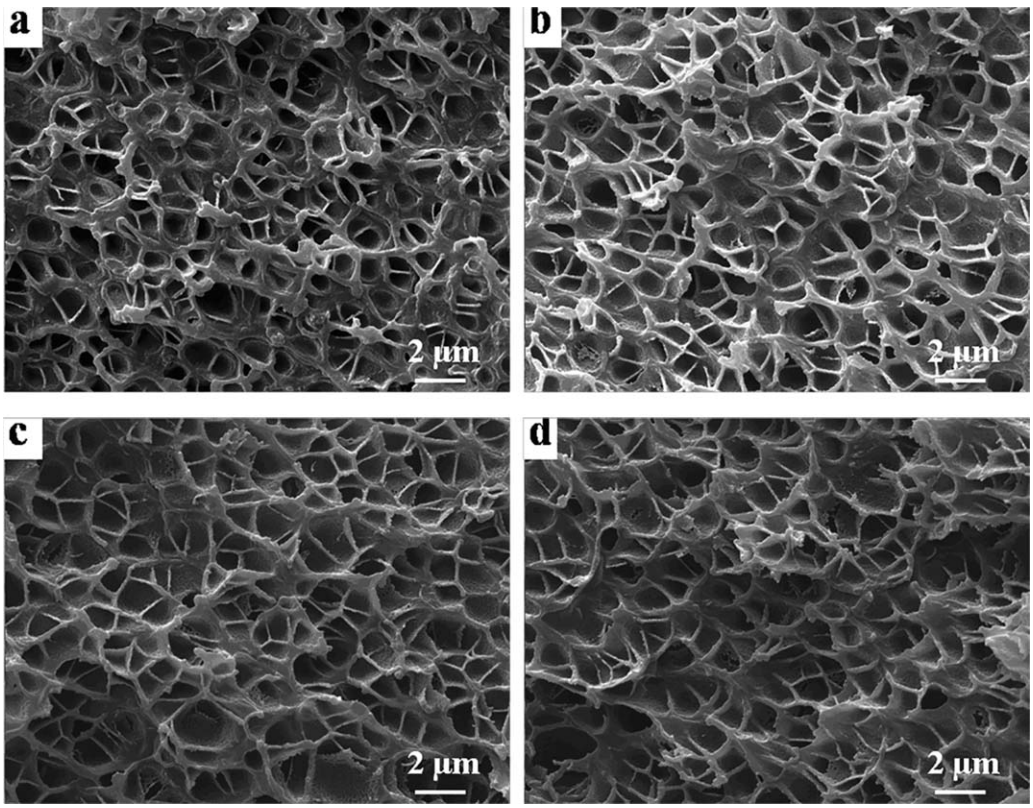

Figure 5. SEM images of the *s*-MWCNT-COOH/PEI nanocomposite foams at 180°C with different foaming times: (a) 5, (b) 15, (c) 25, and (d) 35 s (magnification 6000×, scale bar = 2 μm).

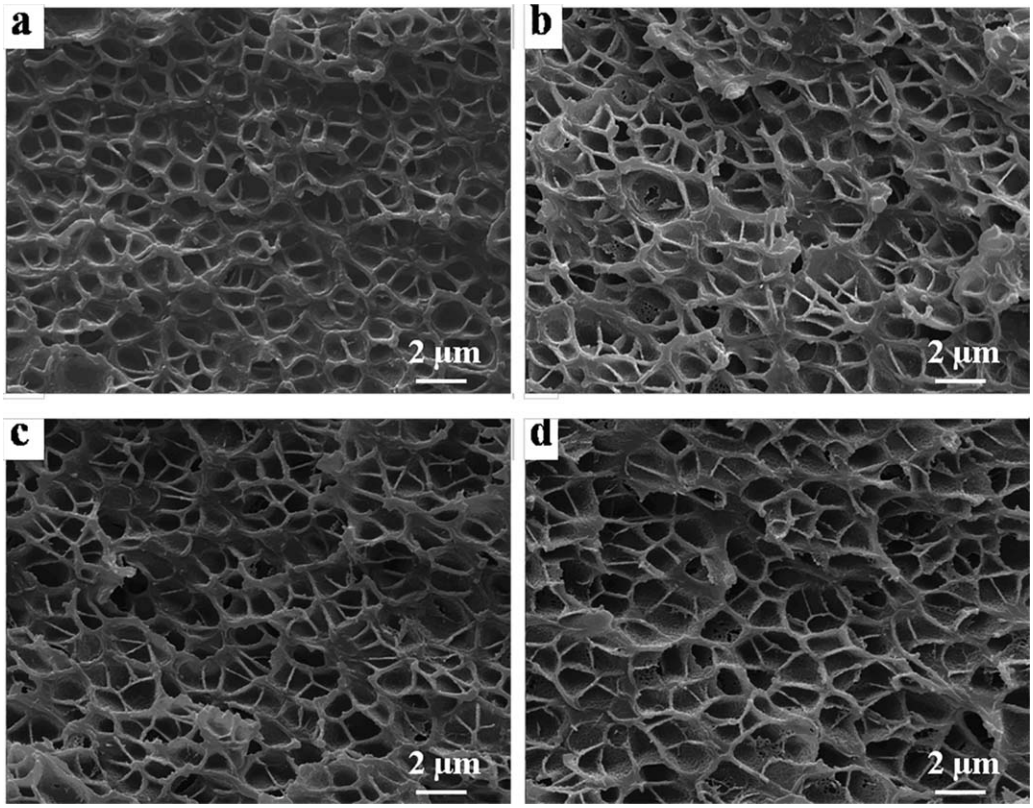

Figure 6. SEM images of the *m*-MWCNT-COOH/PEI nanocomposite foams at 180°C with different foaming times: (a) 5, (b) 15, (c) 25, and (d) 35 s (magnification 6000×, scale bar = 2 μm).

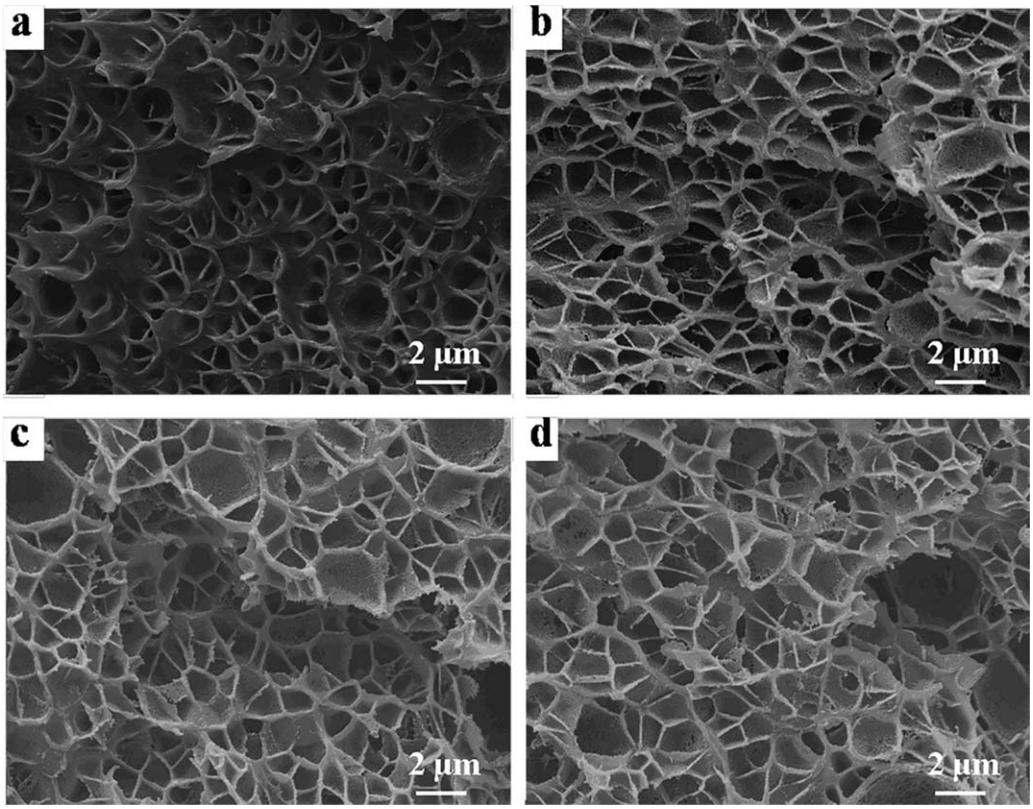

Figure 7. SEM images of the *t*-MWCNT-COOH/PEI nanocomposite foams at 180°C with different foaming times: (a) 5, (b) 15, (c) 25, and (d) 35 s (magnification 6000×, scale bar = 2 μm).

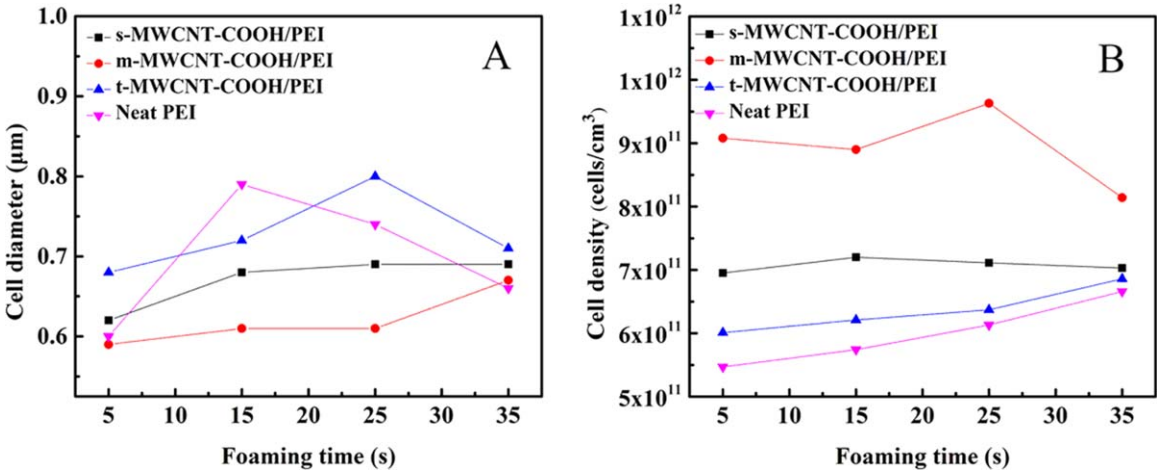

Figure 8. (A) Cell diameter and (B) cell density for the neat PEI and *s*-MWCNT-COOH/PEI, *m*-MWCNT-COOH/PEI, and *t*-MWCNT-COOH/PEI nanocomposite foams prepared with different foaming times. [Color figure can be viewed in the online issue, which is available at wileyonlinelibrary.com.]

the surface energy. The energy reduction factor (f) is a function of the contact angle between the gas bubbles, the nucleation agent, and the relative curvature (w) of the nucleation agent surface to the critical radius (r^*) of the nucleated phase. When a nucleus is in chemical and mechanical equilibrium with its surrounding fluid, it has an r^* that is the minimum nuclei radius needed to grow into a bubble that can be obtained from the following equation:

$$r^* = \frac{2\gamma}{\Delta p} \tag{6}$$

An increase in the nucleus size when it exceeds r^* will lead to a reduction in free energy. Therefore, only nuclei larger than the critical size will grow spontaneously to form stable bubbles.

Because the critical nuclei are extremely small and difficult to observe under experimental or actual processing conditions, the

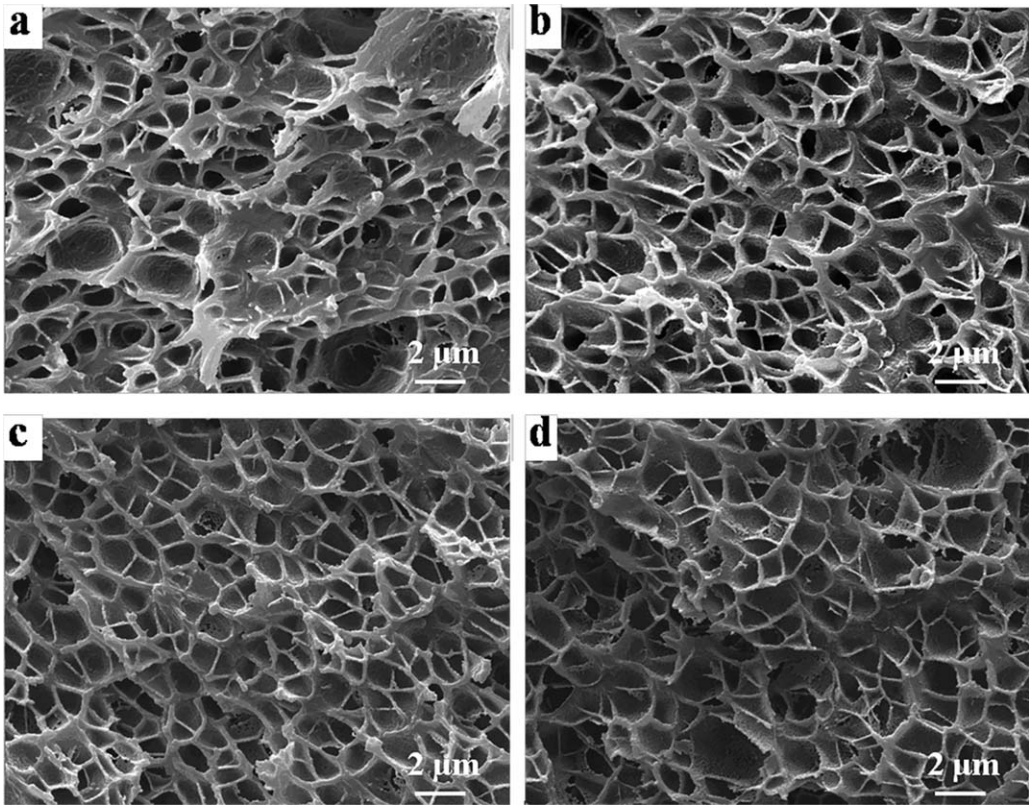

Figure 9. SEM images of the neat PEI and MWCNT-COOH/PEI nanocomposite foams at 180°C for 65 s: (a) neat PEI, (b) *s*-MWCNT-COOH/PEI, (c) *m*-MWCNT-COOH/PEI, and (d) *t*-MWCNT-COOH/PEI (magnification 6000×, scale bar = 2 μm).

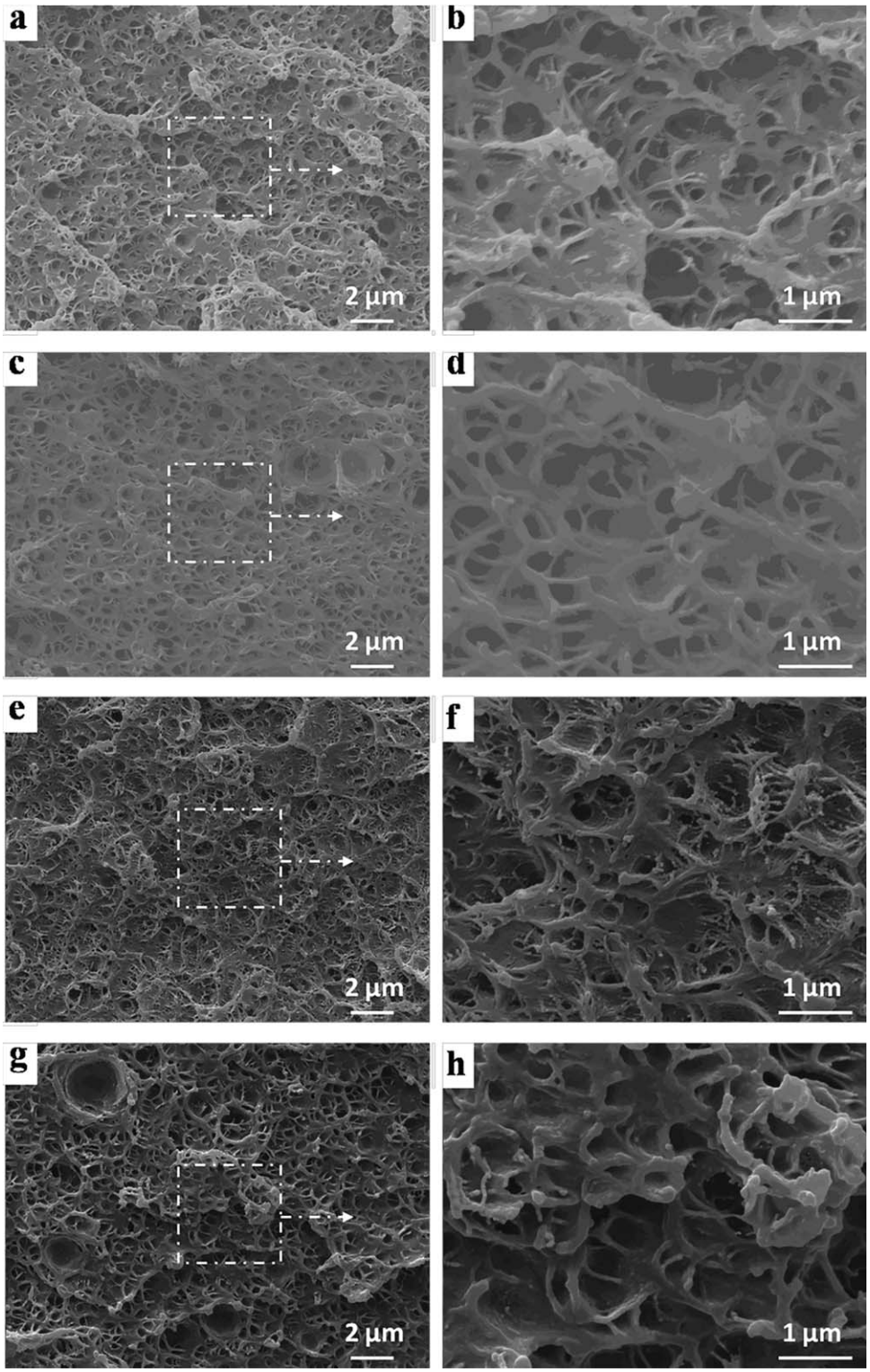

Figure 10. SEM images of the neat PEI and MWCNT-COOH/PEI nanocomposite foams at 170°C for 15 s: (a,b) neat PEI, (c,d) *s*-MWCNT-COOH/PEI, (e,f) *m*-MWCNT-COOH/PEI, and (g,h) *t*-MWCNT-COOH/PEI [(a,c,e,g) magnification 6000× and (b,d,f,h) magnification 20,000×].

calculated value of r^* with density function theory reported for poly(methyl methacrylate) (PMMA)-CO_2 was 2 nm.[27] Costeux and Zhu[28] conceived that the particles with a diameter close to twice r^* could act as a nucleation center and accumulate CO_2 around them, whereas a larger diameter would lead to nuclei forming on a portion of their surface. Thus, one can speculate that in PEI-CO_2 systems, r^* would be approximate to it about 2 nm. In a comparison of the three types of MWCNT-COOHs,

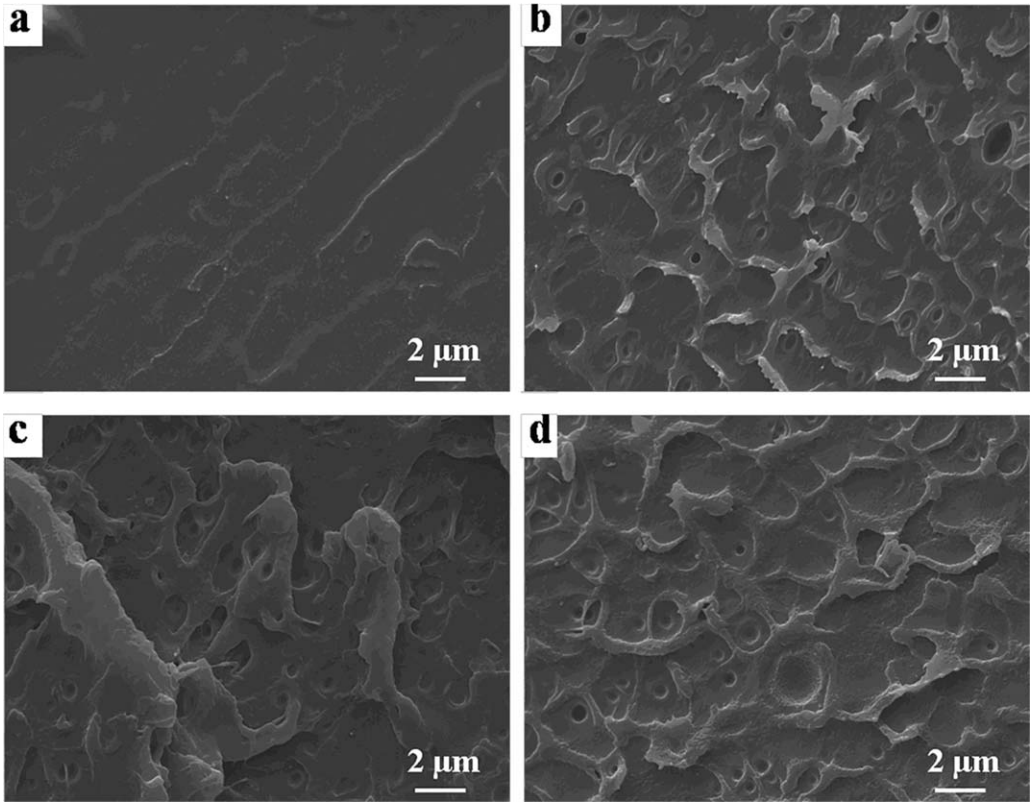

Figure 11. SEM images of the neat PEI foams at 160°C with different foaming times: (a) 5, (b) 15, (c) 25, and (d) 35 s (magnification 6000×, scale bar = 2 μm).

s-MWCNT-COOHs, which had a diameter of less than 8 nm, were theoretically suitable, but they tended to form convex and concave regions around agglomerate and reduced the amount of nucleation sites. Therefore, *m*-MWCNT-COOHs may have been more appropriate as nucleation agents. This was coincident with the experimental results, in which the cell morphology parameter of *m*-MWCNT-COOH/PEI was much better than that of the *s*-MWCNT-COOH/PEI foams. As to the *t*-MWCNT-COOH, the large diameter of nanotubes made the formulated nuclei only on a portion at their surfaces; they then accumulated to form a much bigger cell compared with the *s*-MWCNT-COOH/PEI and *m*-MWCNT-COOH/PEI foams. As a result, the *m*-MWCNT-COOH/PEI foams exhibited the lowest average cell size and the highest cell density.

Influence of the Foaming Time on the Cell Morphology

Figures 4–7 show the effect of the foaming time on the cellular morphology of the MWCNT-COOH/PEI foams at a foaming temperature of 180°C. When the foaming time exceeded 15 s, the cells tended to coalescence and collapse, as shown in these figures; this indicated that the proper foaming time was 15 s. Figure 8 shows the cell morphology parameters of the neat PEI and MWCNT-COOH/PEI foams for different foaming times. As shown in Figure 8, the neat PEI and MWCNT-COOH/PEI foams developed a nanocellular morphology. The cell size of the neat nanocellular PEI foam reached 0.81 μm; this was the largest between the four foams. The cell sizes of the nanocellular *s*-MWCNT-COOH/PEI, *m*-MWCNT-COOH/PEI, and *t*-MWCNT-COOH/PEI foams reached 0.68, 0.61, 0.72 μm. The cell sizes of these nanocellular MWCNT-COOH/PEI foams decreased by 16.05, 24.69, and 11.11%, compared with the neat nanocellular PEI foam, respectively. The cell densities of these nanocellular MWCNT-COOH/PEI foams were higher than that of the neat nanocellular PEI foam. Among them, the nanocellular *m*-MWCNT-COOH/PEI foams had the highest of the cell density, which was 8.9×10^{11} cells/cm^3. We deduced that the MWCNT-COOH nucleation agent improved the number of effective bubble nucleation sites in the MWCNT-COOH/PEI nanocomposites. However, the *m*-MWCNT-COOHs exhibited an excellent heterogeneous nucleation effect because of its proper aspect ratio.

Figure 9 shows the cellular morphology of the neat PEI and MWCNT-COOH/PEI foams at a foaming temperature 180°C for 65 s. As show in Figure 9, the neat PEI foams appeared to coalesce. When MWCNT-COOHs were added under the same conditions, the orientation of MWCNT-COOHs in the PEI matrix protected the cells from destructing during cell growth and suppressed the bubble coalescence; this indicated that the presence of MWCNT-COOH improved the cell structure stability. This was because the melt strength of the MWCNT-COOH/PEI nanocomposites increased with the addition of MWCNT-COOH.[29,30]

Influence of the Foaming Temperature on the Cell Morphology

The foaming temperature is the key parameter determining the cell structure. Figure 10 reveals the cellular morphology of the

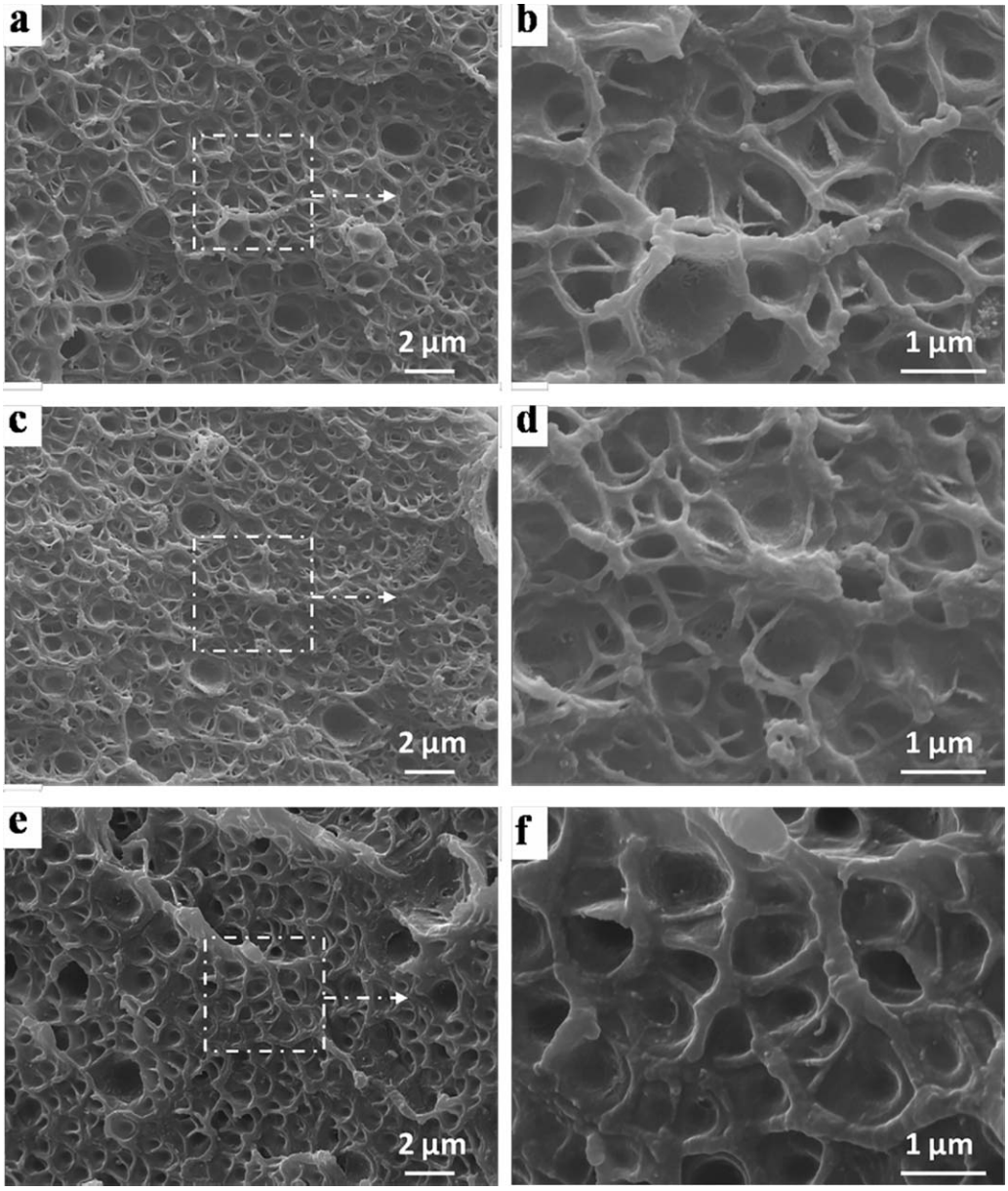

Figure 12. SEM images of the MWCNT-COOH/PEI nanocomposite foams at 160°C for 15 s: (a,b) *s*-MWCNT-COOH/PEI, (c,d) *m*-MWCNT-COOH/PEI, and (e,f) *t*-MWCNT-COOH/PEI [(a,c,e) magnification 6000× and (b,d,f) magnification 20,000×].

neat PEI and MWCNT-COOH/PEI foams at a foaming temperature of 170°C for 15 s. As shown in Figure 10, the cell size became smaller as the foaming temperature decreased from 180 to 170°C, at which the r^* of curvature decreased with decreasing foaming temperature. At higher magnifications, uniform nanocellular structures became visible throughout the cross-sectional areas, and the nanocellular morphologies appeared to be similar to that of microcellular samples with the cells uniformly distributed throughout the volume. Among the three types of nanocomposite foams, the cell size mostly ranged from 100 to 600 nm, but the cell size of the nanocellular *s*-MWCNT-COOH/PEI and *t*-MWCNT-COOH/PEI foams was more or less uneven because of the few microscale foams included. For the neat nanocellular PEI foams, the cell size ranged from 200 to 900 nm, and the cell density decreased compared with that of the nanocellular MWCNT-COOH/PEI foams.

To investigate the effect of the foaming temperature on the cellular morphology, the foaming temperature decreased further. Figure 11 shows the cellular morphology of the neat PEI foams at a foaming temperature of 160°C. As shown in Figure 11, the cell sizes were on the microscale. Meanwhile, at a low foaming temperature, the cell size increased, and the cell density decreased compared with that of foams at high foaming temperatures. With the addition of MWCNT-COOHs, the MWCNT-COOH/PEI foams appeared to be nanoscale foams again; this is shown in Figure 12 and indicated the excellent nucleation effect of these nucleation agents. The effect of the foaming temperature on the average cell diameter, cell density, and bulk density of these foams

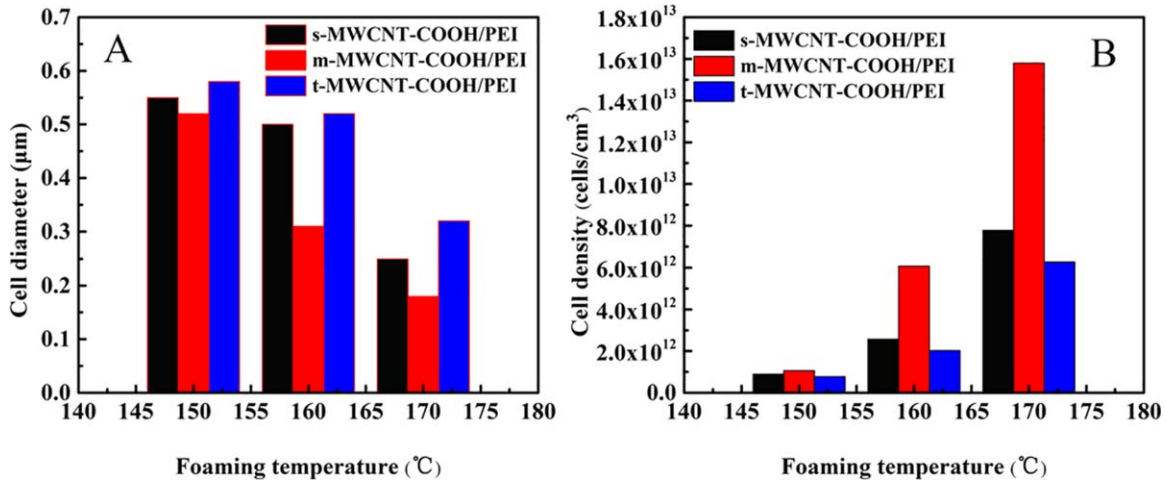

Figure 13. (A) Cell diameter and (B) cell density for the *s*-MWCNT-COOH/PEI, *m*-MWCNT-COOH/PEI, and *t*-MWCNT-COOH/PEI nanocomposite foams prepared at different foaming temperatures. [Color figure can be viewed in the online issue, which is available at wileyonlinelibrary.com.]

Table II. Foam Bulk Density of the Neat PEI and *s*-MWCNT-COOH/PEI, *m*-MWCNT-COOH/PEI, and *t*-MWCNT-COOH/PEI Nanocomposite Foams Prepared at Different Foaming Temperatures with a Foaming Time of 15 s

	Foam bulk density (g/cm^3)			
Foaming temperature (°C)	Neat PEI	s-MWCNT-COOH/PEI	*m*-MWCNT-COOH/PEI	*t*-MWCNT-COOH/PEI
180	0.71	0.67	0.63	0.69
170	0.58	0.54	0.47	0.56
160	1.12	0.83	0.81	0.89

are summarized in Figure 13 and Table II. The nanocellular *m*-MWCNT-COOH/PEI foam had the smallest cell size and highest cell density among all of the nanocellular foams. When the foaming temperature was 170°C, the cell size of the nanocellular *m*-MWCNT-COOH/PEI foams decreased to 180 nm, and the cell density of it increased to 1.58×10^{13} cells/cm^3. Additionally, the bulk density of the nanocomposite foams were even lower than those of the neat PEI foam; this further confirmed the excellent nucleation effect of the nucleation agent. A comparison of the cell morphologies of the nanocellular foams with a higher cell density and smaller cell size; this suggested that the growth of cell density led to a reduction in the amount of CO_2 diffusing into each cell during the bubble growth. Meanwhile, the heterogeneous nucleation agent became more significantly effective at higher foaming temperatures, but the excessive foaming temperature led to the coalescence and collapse of cells because the strength of the matrix decreased with the growth of foaming temperature.

CONCLUSIONS

A series of microcellular PEI foams and nanocellular MWCNT-COOH/PEI foams were prepared by a batch foaming method. MWCNT-COOHs with the different aspect ratios were introduced into the PEI matrix as heterogeneous nucleation agents to improve the cell morphology of microcellular PEI foams. The effects of the aspect ratio of the MWCNT-COOHs on the cellular morphology and gas diffusion were examined. With the addition of MWCNT-COOH, the sorption curve showed a slight reduction in CO_2 solubility, but the gas diffusion rate was improved. Compared with the neat PEI foams, the nanocellular MWCNT-COOH/PEI foams had a smaller average cell size and a higher cell density because of the excellent nucleating efficiency of MWCNT-COOH. Meanwhile, the proper aspect ratio of MWCNT-COOH improved the cellular morphology under the same foaming conditions, which in the *s*-MWCNT-COOH (aspect ratio ≈ 1333) was the best heterogeneous nucleation agent. When the foaming temperature was 170°C, the cell size and cell density of the nanocellular *m*-MWCNT-COOH/PEI foam decreased to 180 nm and increased to 1.58×10^{13} cells/cm^3, respectively.

REFERENCES

1. Baldwin, D. F.; Park, C. B.; Suh, N. P. *Polym. Eng. Sci.* **1996**, *36*, 1437.
2. Seeler, K. A.; Kumar, V. *J. Reinf. Plast. Compos.* **1993**, *12*, 359.
3. Yuan, M.; Turng, L.-S. *Polymer* **2005**, *46*, 7273.
4. Jenkins, M. J.; Harrison, K. L.; Silva, M. M. C. G.; Whitaker, M. J.; Shakesheff, K. M.; Howdle, S. M. *Eur. Polym. J.* **2006**, *42*, 3145.
5. Yuan, M.; Turng, L.-S.; Caulfield, D. F. *Polym. Eng. Sci.* **2006**, *46*, 904.
6. Pilla, S.; Kramschuster, A.; Lee, J.; Auer, G. K.; Gong, S. Q.; Turng, L. S. *Compos. Interface* **2009**, *16*, 869.
7. Pilla, S.; Kim, S. G.; Auer, G. K.; Gong, S.; Park, C. B. *Polym. Eng. Sci.* **2009**, *49*, 1653.

8. Pilla, S.; Kramschuster, A.; Yang, L. Q.; Lee, J.; Gong, S. Q.; Turng, L. S. *Mater. Sci. Eng. C* **2009**, *29*, 1258.
9. Chen, L.; Ozisik, R.; Schadler, L. S. *Polymer* **2010**, *51*, 2368.
10. Yang, J.; Huang, L.; Zhang, Y.; Chen, F.; Fan, P.; Zhong, M.; Yeh, S. *Ind. Eng. Chem. Res.* **2013**, *52*, 14169.
11. Ji, G.; Zhai, W.; Lin, D.; Ren, Q.; Zheng, W.; Jung, D. W. *Ind. Eng. Chem. Res.* **2013**, *52*, 6390.
12. Naguib, H. E.; Park, C. B.; Lee, P. C.; Xu, D. *J. Polym. Eng.* **2006**, *26*, 565.
13. Zhang, C.; Zhu, B.; Lee, L. *J. Polymer* **2011**, *52*, 1847.
14. Coleman, J. N.; Khan, U.; Gun'ko, Y. K. *Adv. Mater.* **2006**, *18*, 689.
15. Coleman, J. N.; Khan, U.; Blau, W. J.; Gun'ko, Y. K. *Carbon* **2006**, *44*, 1624.
16. Zhai, W.; Wang, J.; Chen, N.; Naguib, H. E.; Park, C. B. *Polym. Eng. Sci.* **2012**, *52*, 2078.
17. Ameli, A.; Nofar, M.; Park, C. B.; Pötschke, P.; Rizvi, G. *Carbon* **2014**, *71*, 206.
18. Thess, A.; Lee, R.; Nikolaev, P.; Dai, H.; Petit, P.; Robert, J.; Xu, C.; Lee, Y. H.; Kim, S. G.; Rinzler, A. G.; Colbert, D. T.; Scuseria, G. E.; Tomanek, D.; Fischer, J. E.; Smalley, R. E. *Science* **1996**, *273*, 483.
19. Krause, B.; Sijbesma, H. J. P.; Munuklu, P.; Vegt, N. F. A. V. D.; Wssling, M. *Macromolecules* **2001**, *34*, 8792.
20. Miller, D.; Chatchaisucha, P.; Kumar, V. *Polymer* **2009**, *50*, 5576.
21. Miller, D.; Kumar, V. *Polymer* **2011**, *52*, 2910.
22. Nemoto, T.; Takagi, J.; Ohshima, M. *Polym. Eng. Sci.* **2010**, *50*, 2408.
23. Zhai, W.; Feng, W.; Ling, J.; Zheng, W. *Ind. Eng. Chem. Res.* **2012**, *51*, 12827.
24. Dyke, C. A.; Tour, J. M. *Chem.—Eur. J.* **2004**, *10*, 812.
25. Kazarian, S. G.; Vincent, M. F.; Bright, F. V.; Liotta, C. L.; Eckert, C. A. *J. Am. Chem. Soc.* **1996**, *118*, 1729.
26. Zhou, C.; Vaccaro, N.; Sundarram, S. S.; Li, W. *J. Cell. Plast.* **2012**, *48*, 239.
27. Xu, X.; Cristancho, D. E.; Costeux, S.; Wang, Z. G. Presented at AIChE Annual Meeting, Pittsburgh, PA, *Oct–Nov* **2011**.
28. Costeux, S.; Zhu, L. *Polymer* **2013**, *54*, 2785.
29. Alig, I.; Lellinger, D.; Engel, M.; Skipa, T.; Pötschke, P. *Polymer* **2008**, *49*, 1902.
30. Fujigaya, T.; Nakashima, N. J. *Nanosci. Nanotechnol.* **2012**, *12*, 1717.